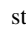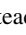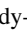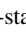# Accurate and fast master equation modeling of triplet-triplet annihilation in organic phosphorescent emission layers including correlations

M. Taherpour ◉, C. van Hoesel ◉, R. Coehoorn ◉, and P. A. Bobbert ◉[*]

Department of Applied Physics and Institute for Complex Molecular Systems, Eindhoven University of Technology,
P.O. Box 513, NL-5600 MB Eindhoven, The Netherlands

Triplet-triplet annihilation (TTA) in phosphorescent emission layers of modern organic light-emitting diodes compromises their performance and device lifetime. TTA can occur by a Förster-type interaction between two triplets, leading to a loss of one of them. The TTA process gives rise to correlations in the positions of the surviving triplets, which complicate its study. These correlations can in principle be accounted for exactly in kinetic Monte Carlo (KMC) simulations, but such simulations are computationally expensive. Here, we present master equation modeling of TTA that accounts for correlations in a computationally efficient way. Cases without and with triplet diffusion, which partly washes out correlations, are considered. We calculate the influence of TTA on transient photoluminescence experiments, where it leads to a deviation from exponential decay, and on steady-state emission efficiency. A comparison with KMC simulations shows that our master equation modeling is an accurate and computationally competitive alternative.

I. INTRODUCTION

The efficiency of organic light-emitting diodes (OLEDs) has dramatically increased due to the introduction of phosphorescent emitters [1]. In these emitters, the spin-orbit coupling induced by a heavy metal atom in the core of the molecule allows fast intersystem crossing (ISC) of singlet to triplet excitons and radiative decay of triplet excitons. As a result, all excitons formed can in principle contribute to phosphorescent emission. At low current densities, the internal quantum efficiency (IQE) of phosphorescent OLEDs approaches 100% [2]. At high current densities, efficiency roll-off occurs, which is mainly attributed to triplet-triplet annihilation (TTA) and triplet-polaron quenching (TPQ) [3–6] ("triplet" will from now on be used as short for "triplet exciton"). Due to these processes, correlations between the positions of the surviving triplets (TTA) and between the positions of charges and surviving triplets (TPQ) will arise. This complicates the evaluation of the effects of TTA and TPQ on the photophysics of phosphorescent OLEDs, and therefore their mitigation. Kinetic Monte Carlo (KMC) simulations provide a mechanistic and therefore in principle exact way to evaluate these effects [7–11]. However, such simulations are computationally expensive.

Recently, Shumilin and Beltukov addressed the problem of the influence of correlations in the positions of charges on single-carrier transport in molecular semiconductors [12]. Such correlations result from the strong Coulomb repulsion of two like charges on the same molecule, which makes occupation of a molecular site by two charges very unlikely. This on-site Coulomb repulsion also leads to correlations in the occupations by charges of different molecular sites, even when the Coulomb repulsion of charges residing on differ-

ent molecules is ignored [12,13]. The approach in Ref. [12] is based on an approximate numerical solution of the hierarchical Bogoliubov-Born-Green-Kirkwood-Yvon (BBGKY) chain of equations [14–16], which is equivalent to a master equation formulation of a system of interacting particles. In this hierarchical chain, the equation of motion for the *n*-particle distribution function has a dependency on the $(n + 1)$-particle distribution function. Solution of the chain of equations therefore requires a closure, which is obtained in Ref. [12] by taking into account covariances in the occupation of molecular sites by charges up to a certain order and neglecting higher-order covariances. In this way, the infinite system of hierarchical equations is truncated to a finite system, which can be solved numerically.

BBGKY-like chains of equations can also be formulated for and applied to the TTA and TPQ processes. However, to the best of our knowledge this has not yet been done. In the present paper, we choose to focus on TTA because of the presence of only one instead of two particle species.

We will assume that TTA is a long-range Förster-type process with an r^{-6} distance dependence between two triplets on phosphorescent guest molecules embedded in a host. In the TTA process, the triplet excitation energy is transferred from a donor molecule carrying the first triplet to the acceptor molecule carrying the second triplet. The Förster-type process that makes this transfer possible is based on the small amount of singlet character mixed in to triplets on the phosphorescent emitter by the spin-orbit coupling that facilitates the phosphorescent emission. After the transfer, the acceptor molecule is in a highly excited triplet state and relaxes thermally to the lowest triplet state, by which the energy of the first triplet is lost. TTA can also occur by Dexter-type processes. However, these processes are only important at very high guest concentrations [17] that are not relevant for efficient phosphorescent OLEDs because of concentration quenching.

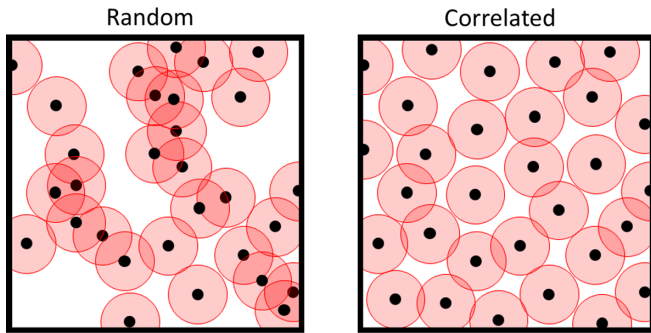[*]Corresponding author: p.a.bobbert@tue.nl

FIG. 1. Sketch of the effect of correlations on triplet positions in the presence of triplet-triplet annihilation (TTA). Left: triplets with random positions (points), as occurring, for example, at the beginning of an experiment where triplets are generated by illumination or in a steady-state situation in the presence of strong triplet diffusion. Right: triplets with correlated positions, occurring as a result of TTA with no or weak diffusion. The circle diameter is a measure for the decay length of the triplet pair correlation function in the correlated case. In both cases, the number of displayed triplets is the same (30).

The correlations in the triplet positions that arise as a result of TTA are illustrated in Fig. 1, which displays two-dimensional sketches of a system with random positions of the triplets (left) and a system with correlated triplet positions (right) that has undergone TTA. Such a situation occurs, for example, in an experiment in which triplets are generated at random positions by illumination, after which they disappear either by radiative decay or TTA. The diameter of the circles drawn around each triplet is a measure for the decay length of the two-triplet, or triplet pair, correlation function. The region inside the circle signifies a triplet depletion zone [8]. A proper description of the resulting structure of a system of positionally correlated surviving triplets requires a many-body treatment. Apart from TTA, we will consider triplet diffusion among the emitters and assume that this diffusion is also a Förster-type process. Diffusion of triplets decreases the correlation established by TTA. Sufficiently strong diffusion will wash out correlations completely [8].

Models for TTA often ignore the positional correlations of triplets. For example, in time-resolved photoluminescence (TRPL) experiments, where triplets are generated at time $t = 0$ by a short light flash, the decay of the time-dependent triplet density $T(t)$ is usually described by the phenomenological equation

$$\frac{dT}{dt} = -k_{\mathrm{r}}T - \frac{1}{2}k_{\mathrm{TTA}}T^2, \tag{1}$$

where k_{r} is the radiative triplet decay rate, and k_{TTA} is a TTA rate coefficient. In previous work, we have shown from KMC simulations that such a description is inaccurate, because it neglects correlations in the positions of surviving triplets [7]. Instead, two effective TTA rate coefficients were introduced to describe a TRPL experiment: a rate coefficient $k_{\mathrm{TTA},1}$ based on the measured time at which half of the emission has taken place and a rate coefficient $k_{\mathrm{TTA},2}$ based on the decrease of the total, time-integrated, photoluminescence (PL) efficiency with respect to the zero-light fluence limit, in which TTA is absent. The ratio $r \equiv k_{\mathrm{TTA},2}/k_{\mathrm{TTA},1}$ is equal to 1 in the strong-

diffusion limit, where Eq. (1) is valid, but the ratio can exceed 2 in the absence of triplet diffusion [7].

In the present paper, we evaluate the effects of TTA in phosphorescent host-guest systems by master equation modeling, including correlations in the triplet positions. Our approach, described in Sec. II, starts by formulating the master equation for the probabilities that the system of triplets is in a particular state. We then derive from this master equation a BBGKY-type hierarchy of equations for the n-triplet distribution functions. Following Ref. [12], we consider a closure of the hierarchy by neglecting covariances beyond a certain order, where we consider in particular the second- and third-order approximation. We find, however, that these approximations are not sufficiently accurate. Much more accurate results are obtained from a low-triplet density or pair approximation (PA) and from an approximation known as the superposition approximation (SA) [18–21].

Readers who are primarily interested in the results of the present work can immediately go to Sec. III. In that section, we present results of our master equation modeling using the various approximations introduced in Sec. II. The results are compared to KMC results, which serve as validation and a benchmark. We consider both the transient case, as occurs in a TRPL experiment, and the steady-state case in which triplets are continuously generated, as occurs in a photoluminescence (PL) experiment with continuous illumination or in OLEDs under stationary operating conditions. In Sec. IV we consider the computational efficiency of our master equation calculations using the PA and SA as compared to KMC simulations. Finally, Sec. V contains a summary, conclusions, and an outlook.

II. METHODS

In this section, we discuss the theoretical and computational methods used in our calculations of triplet-triplet annihilation (TTA). The system that we study represents an emission layer of a phosphorescent organic light-emitting diode (OLED). It consists of a cubic lattice of sites, with a fraction c_{g} of randomly positioned guest sites in an environment of host sites. The guest sites represent phosphorescent molecules that can carry triplets (triplet excitons). The host sites are assumed to be inaccessible to the triplets. For the lattice constant we take $a = 1$ nm, which is a typical value for the intermolecular distance in molecular semiconductors. We neglect in this work energetic disorder, so that there is no energy difference between triplets on different guest sites. Explicit calculations for Ir-cored phosphorescent emitters yield an approximately Gaussian triplet energy disorder with a standard deviation of about 0.05 eV [17], which can be considered, at room temperature, as weak disorder. We consider the following processes: (i) Radiative decay of triplets on the guest sites with a rate $k_{\mathrm{r}} = 1/\tau$, where τ is the radiative triplet lifetime, which is taken to be equal for all sites. We assume here that the nonradiative decay rate is zero, but it is straightforward to extend the present results to a nonzero radiative decay rate. (ii) TTA by a Förster process, governed by a Förster radius $R_{\mathrm{F,TTA}}$, where one of the two triplets involved in the process is annihilated. (iii) Diffusion of triplets between guest sites by a Förster process governed by a Förster

radius $R_{F,diff}$. (iv) Generation of triplets with a generation rate G at random emitter sites that are not yet occupied by a triplet. This generation can take place by illumination, such as in a PL experiment, or by recombination of electrons and holes. We will consider two different situations, corresponding to two types of experiments. In the first situation, we start with a randomly generated configuration of triplets on guest sites, and we study the density $T(t)$ of triplets as a function of time t. This situation is representative of a time-resolved photoluminescence (TRPL) experiment, where a phosphorescent emission layer is illuminated by a short light pulse, after which the luminescence is measured as a function of time. In the second situation, there is a constant generation rate G of triplets, and the steady-state density of triplets T as a function of G is studied. This situation is representative of an experiment under continuous illumination. Also a situation where triplets are generated by electron-hole recombination in an emission layer of an OLED could be described by a constant generation rate G if the likelihood of recombination is approximately the same for all emitter sites.

A. Kinetic Monte Carlo simulations

Our benchmark results are obtained with kinetic Monte Carlo (KMC) simulations [7], performed with the software tool BUMBLEBEE [22]. Simulation boxes of $50 \times 50 \times 50$ sites are used with periodic boundary conditions. The rate S_{ij} for TTA involving two triplets at positions i and j at a mutual distance r_{ij}, where the triplet at i is annihilated, is given by

$$S_{ij} = S(r_{ij}) = \frac{1}{\tau}\left(\frac{R_{F,TTA}}{r_{ij}}\right)^6. \tag{2}$$

The rate D_{ij} for the Förster transfer of a triplet at i to an empty site j is given by

$$D_{ij} = D(r_{ij}) = \frac{1}{\tau}\left(\frac{R_{F,diff}}{r_{ij}}\right)^6. \tag{3}$$

We impose cutoff distances $2R_{F,TTA}$ and $2R_{F,diff}$ on the TTA and diffusion processes beyond which the rates of these processes are taken to be zero. We checked that taking larger cutoffs has no significant influence on the results presented in this work. Since we neglect energy disorder, the TTA and diffusion rates are symmetric: $S_{ij} = S_{ji}$ and $D_{ij} = D_{ji}$. In the presented results, we take averages over 50–300 different simulation runs, depending on the required accuracy. Error bars on the results are indicated when appropriate.

B. General theory

The state of the system is fully specified by the occupations $n_k \in \{0, 1\}$ of all N guest sites by triplets ($k = 1, \ldots, N$). In a master equation approach, one considers the transition rates between all the possible states of the system. The time dependence of the probability $P_\xi(t) \equiv P(n_1, \ldots, n_N; t)$ that the system is at time t in the state ξ with occupations $(n_1, \ldots, n_N)$ is given by the master equation

$$\frac{dP(n_1, \ldots, n_N; t)}{dt} = \sum_{i,j,i \neq j} [-S_{ij}n_i n_j P(n_1, \ldots, n_N; t) + S_{ij}n_i(1 - n_j)P(n_1, \ldots, n_i, \ldots, n_j + 1, \ldots, n_N; t)]$$

$$+ \sum_{i,j,i \neq j} [-D_{ij}n_i(1 - n_j)P(n_1, \ldots, n_N; t) + D_{ij}n_j(1 - n_i)P(n_1, \ldots, n_i + 1, \ldots, n_j - 1, \ldots, n_N; t)]$$

$$+ \sum_i [-k_r n_i P(n_1, \ldots, n_N; t) + k_r(1 - n_i)P(n_1, \ldots, n_i + 1, \ldots, n_N; t)]$$

$$+ \sum_i [-G(1 - n_i)P(n_1, \ldots, n_N; t) + Gn_i P(n_1, \ldots, n_i - 1, \ldots, n_N; t)]. \tag{4}$$

For realistic values of N it is impossible to directly solve these coupled equations for the 2^N probabilities $P_\xi(t)$. Performing KMC simulations is effectively a way to solve these equations. However, obtaining sufficient accuracy for large systems requires long simulation times. Our alternative approach is based on deriving a chain of equations for the n-triplet distribution functions similar to the Bogoliubov-Born-Green-Kirkwood-Yvon (BBGKY) chain of equations [14–16].

We start by defining the one-triplet distribution function

$$\overline{n_k} = \sum_\xi n_{k,\xi} P_\xi(t), \tag{5}$$

where $n_{k,\xi}$ is the occupation number of site k (0 or 1) in state ξ, and where we omit the t-dependence of $\overline{n_k}$. Normalization implies $\sum_\xi P_\xi(t) = 1$. From Eq. (4) in conjunction with Eq. (5)

we can derive for $\overline{n_k}$ the equation

$$\frac{d\overline{n_k}}{dt} = -k_r \overline{n_k} + G(1 - \overline{n_k}) - \sum_{l \neq k} [S_{kl}\overline{n_k n_l} + D_{kl}(\overline{n_k} - \overline{n_l})], \tag{6}$$

where $\overline{n_k n_l}$ is the two-triplet distribution function

$$\overline{n_k n_l} = \sum_\xi n_{k,\xi} n_{l,\xi} P_\xi(t). \tag{7}$$

For the two-triplet distribution function, we can subsequently derive the equation

$$\frac{d\overline{n_k n_l}}{dt} = -2k_r \overline{n_k n_l} - 2S_{kl}\overline{n_k n_l} + G(\overline{n_k} + \overline{n_l} - 2\overline{n_k n_l})$$

$$- \sum_{m \neq k,l} (S_{km} + S_{lm})\overline{n_k n_l n_m} + \sum_{m \neq k,l} [D_{km}(\overline{n_l n_m} - \overline{n_k n_l})$$

$$+ D_{lm}(\overline{n_k n_m} - \overline{n_k n_l})], \tag{8}$$

and for the three-triplet distribution function, we obtain the equation

$$\frac{d\overline{n_k n_l n_m}}{dt} = -3k_r\overline{n_k n_l n_m} - 2(S_{kl} + S_{km} + S_{ml})\overline{n_k n_l n_m} + G(\overline{n_k n_l} + \overline{n_k n_m} + \overline{n_l n_m} - 3\overline{n_k n_l n_m}) - \sum_{p\neq k,l,m} (S_{kp} + S_{lp} + S_{mp})\overline{n_k n_l n_m n_p}$$

$$+ \sum_{p\neq k,l,m} [D_{kp}(\overline{n_l n_m n_p} - \overline{n_k n_l n_m}) + D_{lp}(\overline{n_k n_m n_p} - \overline{n_k n_l n_m}) + D_{mp}(\overline{n_k n_l n_p} - \overline{n_k n_l n_m})]. \tag{9}$$

The complete chain of coupled equations for the *n*-triplet distribution functions of increasing *n* can be written in the following form:

$$\frac{d\overline{\prod_{i\in I} n_i}}{dt} = -k_r|I|\overline{\prod_{i\in I} n_i} - 2\overline{\prod_{i\in I} n_i} \sum_{i,j\in I,j>i} S_{ij} + G\left(\sum_{i\in I}\overline{\prod_{j\in I\setminus i} n_j} - |I|\overline{\prod_{i\in I} n_i}\right)$$

$$- \sum_{j\in I}\sum_{q\notin I}\left(S_{jq}\overline{n_q\prod_{i\in I} n_i}\right) + \sum_{j\in I}\sum_{q\notin I} D_{jq}\left(\overline{n_q\prod_{i\in I\setminus j} n_i} - \overline{\prod_{i\in I} n_i}\right), \tag{10}$$

where $I = \{i_1, i_2, \ldots, i_{|I|}\}$ is an arbitrary set of $|I|$ sites.

Following Ref. [12], we introduce the covariances

$$\overline{\delta n_I} \equiv \overline{\prod_{i\in I}\delta n_i} = \overline{\prod_{i\in I}(n_i - \overline{n_i})} \equiv \sum_{J\subseteq I}(-1)^{|I|-|J|}\left(\overline{\prod_{i\in J} n_i}\prod_{i\in J\setminus I}\overline{n_i}\right), \tag{11}$$

which is a sum with alternating sign over all subsets $J \subseteq I$. Neglecting covariances beyond *m* sites, by putting $\overline{\delta n_I} = 0$ when $|I| \geqslant m + 1$, leads to a closure of Eqs. (10) that we will call the *m*th-order approximation. The mean field (MF), or first-order, approximation corresponds to $m = 1$:

$$\overline{\delta n_k \delta n_l} = \overline{(n_k - \overline{n_k})(n_l - \overline{n_l})} = \overline{n_k n_l} - \overline{n_k}\,\overline{n_l} = 0. \tag{12}$$

With this, Eq. (6) transforms into

$$\frac{d\overline{n_k}}{dt} = -k_r\overline{n_k} + G(1 - \overline{n_k}) - \sum_{l\neq k}[S_{kl}\overline{n_k}\,\overline{n_l} + D_{kl}(\overline{n_k} - \overline{n_l})]. \tag{13}$$

In this work, we will show results obtained with the MF, second-, and third-order approximation. For the second-order approximation, we have

$$\overline{\delta n_k \delta n_l \delta n_m} = \overline{(n_k - \overline{n_k})(n_l - \overline{n_l})(n_m - \overline{n_m})}$$

$$= \overline{n_k n_l n_m} - \overline{n_k n_l}\,\overline{n_m} - \overline{n_k n_m}\,\overline{n_l} - \overline{n_l n_m}\,\overline{n_k} + 2\overline{n_k}\,\overline{n_l}\,\overline{n_m} = 0. \tag{14}$$

So, in the second-order approximation we replace the three-triplet distribution function by lower-order triplet distribution functions:

$$\overline{n_k n_l n_m} \approx \overline{n_k n_l}\,\overline{n_m} + \overline{n_k n_m}\,\overline{n_l} + \overline{n_l n_m}\,\overline{n_k} - 2\overline{n_k}\,\overline{n_l}\,\overline{n_m}. \tag{15}$$

In the third-order approximation, we set $\overline{\delta n_k \delta n_l \delta n_m \delta n_p} = 0$, obtaining

$$\overline{n_k n_l n_m n_p} \approx \overline{n_k n_l n_m}\,\overline{n_p} + \overline{n_k n_l n_p}\,\overline{n_m} + \overline{n_k n_m n_p}\,\overline{n_l} + \overline{n_l n_m n_p}\,\overline{n_k} - \overline{n_k n_l}\,\overline{n_m}\,\overline{n_p} - \overline{n_k n_m}\,\overline{n_l}\,\overline{n_p}$$

$$- \overline{n_k n_p}\,\overline{n_l}\,\overline{n_m} - \overline{n_l n_m}\,\overline{n_k}\,\overline{n_p} - \overline{n_l n_p}\,\overline{n_k}\,\overline{n_m} - \overline{n_m n_p}\,\overline{n_k}\,\overline{n_l} + 3\overline{n_k}\,\overline{n_l}\,\overline{n_m}\,\overline{n_p}. \tag{16}$$

Next to these approximations, we consider two other approximations, which will turn out to be more accurate than the second- and third-order approximations. The first is the pair approximation (PA), which is essentially a low-triplet density approximation. The second is the superposition approximation (SA), where the three-site correlation function is approximated as a product of two-site correlation functions [18–21]. We define the two-site, or pair, correlation function as

$$g_{kl}^{(2)} = \frac{\overline{n_k n_l}}{\overline{n_k}\,\overline{n_l}}, \tag{17}$$

and the three-site correlation function as

$$g_{klm}^{(3)} = \frac{\overline{n_k n_l n_m}}{\overline{n_k}\,\overline{n_l}\,\overline{n_m}}. \tag{18}$$

With these definitions, Eq. (6) becomes

$$\frac{d\overline{n_k}}{dt} = -k_r\overline{n_k} + G(1 - \overline{n_k}) - \sum_{l\neq k}\left(\overline{n_k}\,\overline{n_l}S_{kl}g_{kl}^{(2)} + D_{kl}(\overline{n_k} - \overline{n_l})\right), \tag{19}$$

and Eq. (8) becomes, using Eq. (19),

$$
\frac{dg_{kl}^{(2)}}{dt} = -2S_{kl}g_{kl}^{(2)} + G\left(\frac{1}{\overline{n}_k} + \frac{1}{\overline{n}_l}\right)\left(1 - g_{kl}^{(2)}\right) - \sum_{m\neq k,l}\overline{n}_m(S_{km} + S_{lm})g_{klm}^{(3)} + g_{kl}^{(2)}\left[\sum_{m\neq k}\overline{n}_m S_{km}g_{km}^{(2)} + \sum_{m\neq l}\overline{n}_m S_{lm}g_{lm}^{(2)}\right]
$$
$$
+ g_{kl}^{(2)}D_{kl}\left(2 - \frac{\overline{n}_l}{\overline{n}_k} - \frac{\overline{n}_k}{\overline{n}_l}\right) - g_{kl}^{(2)}\sum_{m\neq k,l}\overline{n}_m\left(\frac{1}{\overline{n}_k}D_{km} + \frac{1}{\overline{n}_l}D_{lm}\right) + \sum_{m\neq k,l}\overline{n}_m\left(\frac{1}{\overline{n}_k}D_{km}g_{lm}^{(2)} + \frac{1}{\overline{n}_l}D_{lm}g_{km}^{(2)}\right). \tag{20}
$$

In the low-triplet density limit, we can neglect in Eq. (20) the third and fourth terms, because they are of higher order in the triplet density than the other terms. This leads to

$$
\frac{dg_{kl}^{(2)}}{dt} = -2S_{kl}g_{kl}^{(2)} + G\left(\frac{1}{\overline{n}_k} + \frac{1}{\overline{n}_l}\right)\left(1 - g_{kl}^{(2)}\right) + g_{kl}^{(2)}D_{kl}\left(2 - \frac{\overline{n}_l}{\overline{n}_k} - \frac{\overline{n}_k}{\overline{n}_l}\right)
$$
$$
- g_{kl}^{(2)}\sum_{m\neq k,l}\overline{n}_m\left(\frac{1}{\overline{n}_k}D_{km} + \frac{1}{\overline{n}_l}D_{lm}\right) + \sum_{m\neq k,l}\overline{n}_m\left(\frac{1}{\overline{n}_k}D_{km}g_{lm}^{(2)} + \frac{1}{\overline{n}_l}D_{lm}g_{km}^{(2)}\right). \tag{21}
$$

We call this the pair approximation because in the low-triplet density limit, the situation with the lowest density where there is still TTA is that of a pair of two triplets.

In the superposition approximation, one assumes that the correlation between three interacting particles (in our case triplets) arises from independent pair interactions between these particles (in our case the TTA process) [18–21,23]. Adopting this approximation, the three-site correlation function $g_{klm}^{(3)}$ in Eq. (20) is approximated as $g_{klm}^{(3)} \approx g_{kl}^{(2)}g_{km}^{(2)}g_{lm}^{(2)}$. Using the SA in Eq. (20) yields

$$
\frac{dg_{kl}^{(2)}}{dt} = -2S_{kl}g_{kl}^{(2)} + G\left(\frac{1}{\overline{n}_k} + \frac{1}{\overline{n}_l}\right)\left(1 - g_{kl}^{(2)}\right) - g_{kl}^{(2)}\sum_{m\neq k,l}\overline{n}_m(S_{km} + S_{lm})g_{km}^{(2)}g_{lm}^{(2)} + g_{kl}^{(2)}\left[\sum_{m\neq k}\overline{n}_m S_{km}g_{km}^{(2)} + \sum_{m\neq l}\overline{n}_m S_{lm}g_{lm}^{(2)}\right]
$$
$$
+ g_{kl}^{(2)}D_{kl}\left(2 - \frac{\overline{n}_l}{\overline{n}_k} - \frac{\overline{n}_k}{\overline{n}_l}\right) - g_{kl}^{(2)}\sum_{m\neq k,l}\overline{n}_m\left(\frac{1}{\overline{n}_k}D_{km} + \frac{1}{\overline{n}_l}D_{lm}\right) + \sum_{m\neq k,l}\overline{n}_m\left(\frac{1}{\overline{n}_k}D_{km}g_{lm}^{(2)} + \frac{1}{\overline{n}_l}D_{lm}g_{km}^{(2)}\right). \tag{22}
$$

We can solve Eqs. (21) and (22) for $g_{kl}^{(2)}$ in conjunction with Eq. (19) to obtain results in the PA and SA, respectively.

C. No triplet diffusion

We first discuss the case without triplet diffusion by putting $D_{kl} = 0$ in the equations of the previous subsection. If there is no diffusion and the guest sites are randomly distributed, all sites become equivalent after performing an average over all possible distributions of guest and host sites. We then no longer need to distinguish between guest and host sites, so that we can exploit the full symmetry of the lattice. Using translational symmetry, we can put $\overline{n}_k = \overline{n}_0 \equiv n(t)$ for all k, where we choose a relabeling such that $k = 0$ is the site at the origin. We are interested in calculating the triplet density $T(t) = n(t)/a^3$, which can be obtained by transforming Eq. (19) into

$$
\frac{dT}{dt} = -k_r T + G\left(\frac{1}{a^3} - T\right) - T^2 a^3 \sum_{l\neq 0} S(r_{0l})g(r_{0l}, t), \tag{23}
$$

with

$$
g(r_{kl}, t) \equiv g_{kl}^{(2)}, \tag{24}
$$

where because of the above-mentioned lattice symmetry, the pair correlation function now only depends on the distance r_{kl} between two sites k and l.

We start by considering a transient situation with no generation of triplets, $G = 0$, describing a TRPL experiment. At

time $t = 0$ we have a density T_0 of randomly placed triplets with uncorrelated positions. The MF expression for T is obtained by neglecting correlations and is equivalent to Eq. (1). It follows by putting $g(r_{0l}, t) = 1$ in Eq. (23):

$$
\frac{dT}{dt} = -k_r T - \frac{1}{2}k_{TTA}T^2, \tag{25}
$$

with the MF TTA rate coefficient defined by

$$
k_{TTA} \equiv 2\times 8.402\, k_r \frac{R_{F,TTA}^6}{a^3}, \tag{26}
$$

where we performed the three-dimensional (3D) lattice sum

$$
a^6 \sum_{l\neq 0}\frac{1}{r_{0l}^6} = 8.402. \tag{27}
$$

Equation (25) can be solved analytically, yielding [24]

$$
T(t) = \frac{k_r T_0}{\left(k_r + \frac{1}{2}k_{TTA}T_0\right)\exp(k_r t) - \frac{1}{2}k_{TTA}T_0}. \tag{28}
$$

We will also consider the two-dimensional (2D) equivalent of these results. The 2D equivalent of the lattice sum in Eq. (27) has the value 4.659. Equation (25) remains the same, where T is now expressed in nm^{-2} with $k_{TTA} \equiv 2\times 4.659 R_{F,TTA}^6/a^4$.

In the second-order approximation we solve Eqs. (6) and (8), using the approximation Eq. (15) in the latter equation. In the third-order approximation we include Eq. (9) in addition to Eqs. (6) and (8), and we use the approximation Eq. (16). In both cases, we cut off the system of equations by only

considering TTA for sites separated by a distance smaller than $2R_{F,TTA}$, as in the KMC simulations. Equivalently, we replace distribution functions of second and third order by lower-order distribution functions when two sites are farther apart than $2R_{F,TTA}$, where the first-order distribution function is $n(t)$. We checked that with this procedure, sufficient accuracy is obtained in the presented results. We exploit the point-group symmetry of the cubic lattice to further reduce the number of equations. The resulting finite system of coupled time-dependent differential equations is solved with standard numerical techniques, using as a boundary condition at $t = 0$ distribution functions corresponding to an uncorrelated situation.

Turning to the PA, Eq. (21) becomes, putting $D_{kl} = G = 0$ and using Eq. (24),

$$\frac{dg(r_{0l}, t)}{dt} = -2S(r_{0l})g(r_{0l}, t), \qquad (29)$$

which leads, with $g(r_{0l}, t = 0) = 1$, to

$$g(r_{0l}, t) = \exp\left[-2k_r t\left(\frac{R_{F,TTA}}{r_{0l}}\right)^6\right]. \qquad (30)$$

Inserting this into Eq. (23), we obtain, with $G = 0$,

$$\frac{dT}{dt} = -k_r T - T^2 a^3 \sum_{l \neq 0} S(r_{0l})g(r_{0l}, t). \qquad (31)$$

In very good approximation, we can replace the lattice sum in this equation by an integral, which can be performed analytically:

$$\sum_{l \neq 0} S(r_{0l})g(r_{0l}, t) \approx \frac{k_r}{a^3} \int d\mathbf{r} \left(\frac{R_{F,TTA}}{r}\right)^6$$

$$\times \exp\left[-2tk_r\left(\frac{R_{F,TTA}}{r}\right)^6\right]$$

$$= \frac{\sqrt{2}}{3} \pi^{\frac{3}{2}} \left(\frac{R_{F,TTA}}{a}\right)^3 \sqrt{\frac{k_r}{t}}. \qquad (32)$$

With this Eq. (31) can be solved, resulting in

$$T(t) = \frac{T_0 e^{-k_r t}}{1 + \frac{\sqrt{2}}{3}\pi^2 R_{F,TTA}^3 T_0 \operatorname{erf}(\sqrt{k_r t})}. \qquad (33)$$

This result is equal to Eq. (17) in Ref. [25] (with the replacement $1/3 \rightarrow \sqrt{2}/3$ in the denominator of that equation) and to Eq. (5) in Ref. [9] with $b = 1/\sqrt{2}$.

Using the 2D equivalent of the integral in Eq. (32), we get

$$\sum_{l \neq 0} S(r_{0l})g(r_{0l}, t) \approx \frac{\pi \Gamma\left(\frac{2}{3}\right)}{3 \, 2^{2/3}} \left(\frac{R_{F,TTA}}{a}\right)^2 \frac{k_r^{1/3}}{t^{2/3}}, \qquad (34)$$

yielding the following 2D equivalent of Eq. (33) for the PA transient:

$$T(t) = \frac{T_0 e^{-k_r t}}{1 + \frac{2^{1/3}}{6} T_0 R_{F,TTA}^2 \pi \Gamma\left(\frac{2}{3}\right)\left[\Gamma\left(\frac{1}{3}\right) - \Gamma\left(\frac{1}{3}, k_r t\right)\right]}, \qquad (35)$$

with $\Gamma(z)$ the Euler Gamma function and $\Gamma(b, z)$ the upper incomplete Gamma function.

Finally, in the SA we obtain from Eq. (22)

$$\frac{dg(r_{0l}, t)}{dt} = -2S(r_{0l})g(r_{0l}, t) - Ta^3 \sum_{m \neq 0, l} [S(r_{0m}) + S(r_{lm})]$$

$$\times g(r_{0l}, t)g(r_{0m}, t)g(r_{lm}, t)$$

$$+ 2Ta^3 g(r_{0l}, t) \sum_{m \neq 0} S(r_{0m})g(r_{0m}, t). \qquad (36)$$

Numerically solving this equation in conjunction with Eq. (23) yields the SA results. The numerical procedure we used is similar to that used for the second- and third-order approximation.

We now consider the steady-state situation, where we are interested in the steady-state triplet density T as a function of the triplet generation rate G. The MF result is obtained by putting $dT/dt = 0$ and $g(r_{0l}, t) = 1$ in Eq. (23), which leads to

$$T(G) = \frac{\sqrt{(G + k_r)^2 + 2Gk_{TTA}/a^3} - (G + k_r)}{k_{TTA}}. \qquad (37)$$

The steady state results in the second- and third-order approximation are obtained in the same way as in the transient case, but now with the inclusion of the terms containing G. We numerically solve the coupled system of time-dependent differential equations until no further change in time is observed. The results are independent of the choice of the initial distribution functions at $t = 0$. The presented results are obtained with distribution functions that initially correspond to an uncorrelated situation.

In the PA, Eq. (21) becomes in the steady state, with $D_{kl} = 0$,

$$-2S(r_{0l})g(r_{0l}) + \frac{2G}{Ta^3}[1 - g(r_{0l})] = 0, \qquad (38)$$

which leads to

$$g(r_{0l}) = \frac{1}{1 + \frac{Ta^3 S(r_{0l})}{G}}. \qquad (39)$$

Inserting this into Eq. (23) and putting $dT/dt = 0$, we obtain

$$-k_r T + G\left(\frac{1}{a^3} - T\right) - T^2 a^3 \sum_{l \neq 0} \frac{GS(r_{0l})}{G + Ta^3 S(r_{0l})} = 0. \qquad (40)$$

We can, again in very good approximation, replace the lattice sum by an integral:

$$\sum_{l \neq 0} \frac{GS(r_{0l})}{G + Ta^3 S(r_{0l})} \approx \frac{Gk_r}{a^3} \int d\mathbf{r} \left(\frac{R_{F,TTA}}{r}\right)^6$$

$$\times \frac{1}{G + Ta^3 k_r \left(\frac{R_{F,TTA}}{r}\right)^6}$$

$$= \frac{2}{3}\sqrt{\frac{Gk_r}{Ta^3}} \pi^2 \left(\frac{R_{F,TTA}}{a}\right)^3, \qquad (41)$$

so that Eq. (40) becomes

$$-k_r T + G\left(\frac{1}{a^3} - T\right) - \frac{2}{3}T^{3/2} a^{3/2} \pi^2 \sqrt{Gk_r} \left(\frac{R_{F,TTA}}{a}\right)^3$$

$$= 0. \qquad (42)$$

This equation can easily be solved numerically to obtain $T(G)$. The 2D equivalent of the lattice sum Eq. (41) is

$$\sum_{l \neq 0} \frac{GS(r_{0l})}{G + Ta^3 S(r_{0l})} = \frac{2}{3\sqrt{3}} \left(\frac{G^2 k_r}{T^2 a^4} \right)^{1/3} \pi^2 \left(\frac{R_{F,TTA}}{a} \right)^2, \quad (43)$$

so that the 2D equivalent of Eq. (42) for the steady-state PA triplet density becomes

$$-k_r T + G \left(\frac{1}{a^2} - T \right) - \frac{2}{3\sqrt{3}} T^{4/3} a^{2/3} \pi^2 (G^2 k_r)^{1/3} \left(\frac{R_{F,TTA}}{a} \right)^2$$
$$= 0. \quad (44)$$

In the SA, Eq. (22) becomes in the steady state, with $D_{kl} = 0$,

$$-2S(r_{0l})g(r_{0l}) + \frac{2G}{Ta^3}[1 - g(r_{0l})]$$
$$- Ta^3 \sum_{m \neq 0,l} [S(r_{0m}) + S(r_{lm})]g(r_{0l})g(r_{0m})g(r_{lm})$$
$$+ 2Ta^3 g(r_{0l}) \sum_{l \neq 0} S(r_{0l})g(r_{0l}) = 0. \quad (45)$$

In principle, this equation can be solved directly, in conjunction with Eq. (23) after putting $dT/dt = 0$. Instead, we use the same practical approach as for the second- and third-order approximation, and we solve the corresponding time-dependent coupled differential equations until no further change in time is observed.

D. Triplet diffusion

In this subsection, we include diffusion of triplets. We will no longer consider for this case the second- and third-order approximation, since we will see in the next section that for the case without diffusion, these approximations turn out to be considerably less accurate than the PA and SA.

Since diffusion of triplets can only occur among guest sites, we encounter the problem of percolation, where fast triplet diffusion can occur along percolating pathways of guest sites that happen to be close together. This is a problem that we cannot fully address without sacrificing translational symmetry. Instead, we preserve translational symmetry and use an approximate approach, which is based on the idea that the fraction of sites available for diffusion is c_g and that the typical minimal distance over which triplet transfer can occur is therefore $c_g^{-1/3} a$ instead of a. This approximation neglects the fact that there can be percolating pathways for triplet transfer with nearest-neighbor guest sites closer than this distance. Therefore, our approach will underestimate triplet diffusion. However, because of the long-range character of the Förster transfer, this underestimation is not severe. The other approximation we make is the replacement of the lattice description by a continuum description. In this continuum description, the discreteness of the underlying lattice is reflected by a minimal distance r_0 of the order of the lattice constant a over which TTA can occur, which is the same as in the case of no diffusion. We choose the value of r_0 such that Förster-type sums can be replaced by corresponding integrals:

$$a^6 \sum_{l \neq 0} \frac{1}{r_{0l}^6} = 4\pi a^3 \int_{r_0}^{\infty} dr \, r^2 \frac{1}{r^6} = \frac{4\pi}{3} \left(\frac{a}{r_0} \right)^3 = 8.402, \quad (46)$$

where we have performed the same lattice sum as in Eq. (27). From this we find $r_0 = 0.7929a$. Accordingly, a minimal distance $\tilde{r}_0 = c_g^{-1/3} r_0$ is introduced over which triplet transfer can take place. With the above approximations, Eq. (19) transforms into

$$\frac{dT}{dt} = -k_r T + G \left(\frac{1}{a^3} - T \right) - 4\pi T^2 \int_{r_0}^{\infty} dr \, r^2 S(r)g(r,t). \quad (47)$$

In the MF approximation, we have $g(r,t) = 1$ and we obtain exactly the same results as without diffusion, discussed in the previous subsection, both in the transient and steady-state case and irrespective of the guest fraction c_g. The PA for the two-triplet correlation function Eq. (21) turns into

$$\frac{dg(r,t)}{dt} = -2S(r)g(r,t) + \frac{2G}{Ta^3}[1 - g(r,t)]$$
$$- 2g(r,t) \frac{c_g}{a^3} \int_{V \setminus \delta \tilde{V}_0 \setminus \delta V_r} d\mathbf{r}' D(r')$$
$$+ 2 \frac{c_g}{a^3} \int_{V \setminus \delta \tilde{V}_0 \setminus \delta V_r} d\mathbf{r}' D(r')g(|\mathbf{r}' - \mathbf{r}|,t), \quad (48)$$

where $\setminus \delta V_r$ and $\setminus \delta \tilde{V}_r$ indicate that a spherical volume with a radius r_0 and $\tilde{r}_0$, respectively, around $\mathbf{r}$ is excluded from the integrals over the infinite volume V. The last two terms have a prefactor c_g because the density of sites available for diffusion is reduced by that factor. The SA Eq. (22) becomes

$$\frac{dg(r,t)}{dt} = -2S(r)g(r,t) + \frac{2G}{Ta^3}[1 - g(r,t)]$$
$$+ 2Tg(r,t) \int_{V \setminus \delta V_0} d\mathbf{r}' S(r')g(r',t)$$
$$- Tg(r,t) \int_{V \setminus \delta V_0 \setminus \delta V_r} d\mathbf{r}' [S(r') + S(|\mathbf{r}' - \mathbf{r}|)]$$
$$\times g(r',t)g(|\mathbf{r}' - \mathbf{r}|,t)$$
$$- 2g(r,t) \frac{c_g}{a^3} \int_{V \setminus \delta \tilde{V}_0 \setminus \delta V_r} d\mathbf{r}' D(r')$$
$$+ 2 \frac{c_g}{a^3} \int_{V \setminus \delta \tilde{V}_0 \setminus \delta V_r} d\mathbf{r}' D(r')g(|\mathbf{r}' - \mathbf{r}|,t). \quad (49)$$

We obtain transient results from Eqs. (47) and (48) (PA) or (49) (SA) by setting $G = 0$ and solving the resulting equations numerically, where the integrals are evaluated using a spectral method. For numerical reasons, we set the pair correlation function $g(r,t) = 1$ when $r \geqslant 250$ nm, which means that we neglect correlations for larger distances. We checked that this is a sufficiently large cutoff on the correlations. Steady-state results are obtained by including the terms including G and solving the equations until no further change in time is observed, as we did for the case without diffusion.

III. RESULTS

A. No triplet diffusion

In this subsection, we discuss the impact of triplet correlations on TTA in TRPL experiments and steady-state conditions in the absence of triplet diffusion. In the simulation of TRPL experiments, the triplets are initially randomly
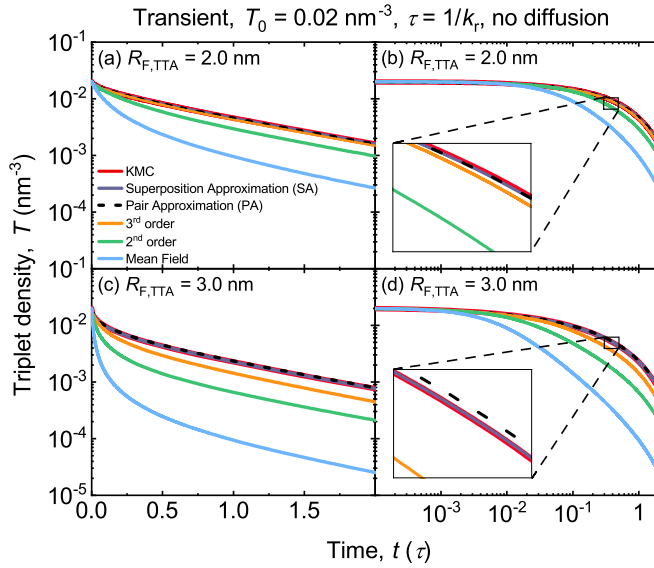
FIG. 2. Transient triplet density $T(t)$ in a simulation of a TRPL experiment with an initial triplet density $T_0 = 0.02$ nm^{-3}, in the absence of triplet diffusion. (a) Transients for the various approximations discussed in Sec. II as compared to KMC results, for $R_{F,TTA} = 2.0$ nm. (b) Same as (a), but with a logarithmic time axis. (c) and (d) Same as (a) and (b), but for $R_{F,TTA} = 3.0$ nm. The insets in (b) and (d) are magnifications of the indicated regions.

FIG. 3. Transient triplet density for $R_{F,TTA} = 3.0$ nm and different initial triplet densities $T_0 = 10^{-3}$, 2×10^{-3}, 5×10^{-3}, 10^{-2}, and 2×10^{-2} nm^{-3}, in the absence of triplet diffusion. Transients are shown for the four main approximations: (a) second order, (b) third order, (c) PA, and (d) SA, in comparison to KMC transients.

positioned. In the absence of triplet diffusion, the value of the guest concentration is then irrelevant, because also the positions of the phosphorescent guest molecules are taken to be random. In steady-state conditions, we assume that there is a constant generation rate of triplets, which occurs randomly at guest molecules that are not yet occupied by another triplet.

Figure 2 shows the time-dependent triplet density $T(t)$ in simulations of a TRPL experiment with an initial triplet density $T_0 = 0.02$ nm^{-3} for two different TTA Förster radii $R_{F,TTA} = 2.0$ nm (top graphs) and 3.0 nm (bottom graphs). For a typical phosphorescent guest concentration of 10%, $T_0 = 0.02$ nm^{-3} corresponds to 20% initial occupation of the guest molecules by a triplet. The time t is expressed in units of the triplet lifetime $\tau = 1/k_r$. The measured photoluminescence is proportional to $T(t)$. We show transients up to $t = 2\tau$, which is a typical time range in TRPL experiments. Figures 2(a) and 2(c) are semilog, and 2(b) and 2(d) are log-log plots of the same data. We compare the transients for the five approximations discussed in Sec. II B to those of KMC simulations discussed in Sec. II A, which serve as a benchmark. The MF and PA transients are given by the analytical expressions Eqs. (28) and (33), respectively.

The effect of TTA is clearly seen in all transients from the nonexponential decay. After some time, triplets that are initially close to each other will have undergone TTA, creating correlations in the positions of the triplets as sketched in Fig. 1(b). For long times, the surviving triplets become isolated and TTA ceases to be important, as observed by the exponential decay at long times, as most clearly visible in Figs. 2(a) and 2(c). We see that the MF transients, obtained from Eq. (28), start to strongly deviate from the KMC transients after $t \approx 10^{-2}\tau$ for $R_{F,TTA} = 2.0$ nm and $t \approx 10^{-3}\tau$

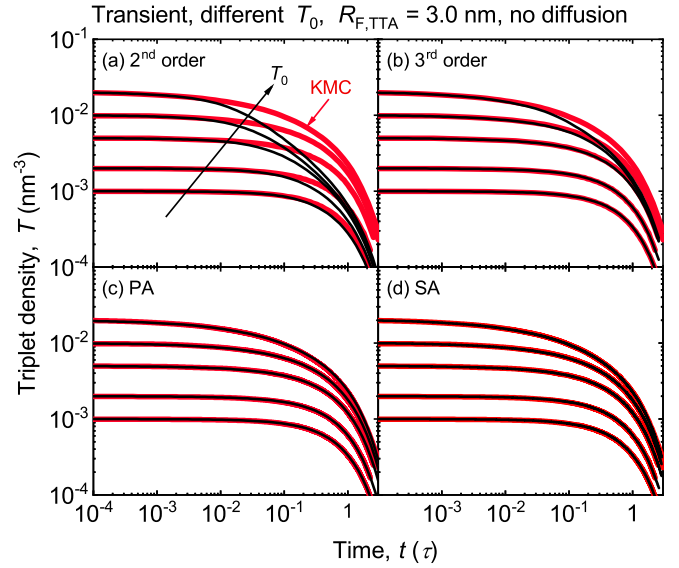for $R_{F,TTA} = 3.0$ nm; see Figs. 2(b) and 2(d), respectively. The reason for the deviation is that correlations in the positions of the triplets are neglected in the MF approximation, which leads to an overestimation of TTA and a too strong initial decrease of $T(t)$. The second- and third-order transients are increasingly accurate, but even the third-order transients finally deviate considerably from the KMC transients. On the other hand, the transients for the PA and the SA follow the KMC transients quite accurately. The magnification in Fig. 2(d) shows that for $R_{F,TTA} = 3.0$ nm and times approaching $t = \tau$ a small deviation of the PA from the KMC transient becomes visible, while the SA transient still closely follows the KMC transient. The magnification in Fig. 2(b) shows that for $R_{F,TTA} = 2.0$ nm also the PA transient keeps on following the KMC transient quite closely.

Figure 3 shows, for $R_{F,TTA} = 3.0$ nm and different initial triplet densities T_0 between 10^{-3} and 2×10^{-2} nm^{-3}, transients for the second- and third-order approximations and for the PA and SA, in comparison to the KMC transients. We see that the second- and third-order transients deviate less from the KMC transients at lower T_0, which is related to the fact that at lower initial triplet densities, correlation effects are less important. As expected, the third-order transients are superior to the second-order transients. The PA and SA transients follow the KMC transients very closely for all values of T_0.

In Fig. 4 we show the triplet pair correlation function $g(r, t)$ [Eq. (24)] at various distances r as a function of t for $R_{F,TTA} = 3.0$ nm and a high initial triplet density of $T_0 = 2 \times 10^{-2}$ nm^{-3}, for which the effects of TTA are relatively strong. We show results for the same approximations as in Fig. 3, in comparison to KMC results. The values of r correspond to the possible distances between points of the used cubic lattice with lattice constant $a = 1$ nm. Initially, we have $g(r, t = 0) = 1$, which expresses the fact that the triplets are initially randomly
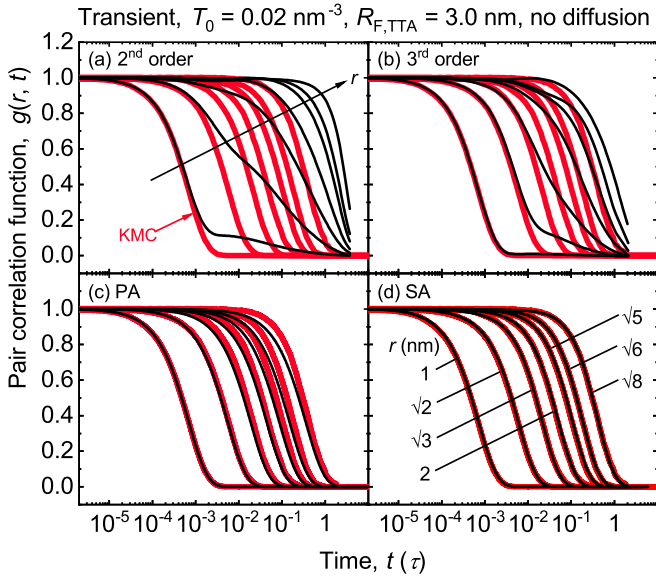
FIG. 4. Triplet pair correlation function $g(r, t)$ in the absence of triplet diffusion as a function of time at various distances r for $R_{F,TTA} = 3.0$ nm and $T_0 = 0.02$ nm^{-3}. Results are shown for the four main approximations, (a) second order, (b) third order, (c) PA, and (d) SA, in comparison to KMC results.

positioned without any correlation. When time proceeds, a depletion zone with a radius of about $R_F(2k_r t)^{1/6}$ [see Eq. (30)] develops around each triplet by the TTA process [8], where the probability of finding another triplet is reduced. Finally, $g(r, t)$ becomes zero for all r, which happens at a later time for larger r, indicating the presence of a growing fully developed depletion zone. The accuracy with which the transients of the various approximations in Fig. 3 follow the KMC transients is reflected in the accuracy with which the corresponding correlation functions follow the KMC correlation function. The PA correlation function in Fig. 4(c), given by Eq. (30), is a substantial improvement to the second-order [Fig. 4(a)] and third-order [Fig. 4(b)] correlation functions, yielding only small deviations from the KMC correlation function at long distances. The SA correlation function in Fig. 4(d) shows an excellent agreement.

We now turn to the steady-state situation where triplets are generated randomly, at positions where there is no other triplet, with a rate G. This corresponds to an experiment under continuous illumination or to the situation where triplets are homogeneously generated by electron-hole recombination in an emission layer of an OLED. In the latter case, we neglect the interaction of the triplets with the electrons and holes.

In Figs. 5(a) and 5(b) we show the steady-state triplet density T as a function of the generation rate G for $R_{F,TTA} =$ 2.0 and 3.0 nm, respectively, for the five approximations of Sec. II B, in comparison to KMC results. The MF result is given by the analytical expression Eq. (37). The PA result is obtained by solving the analytical expression Eq. (42). For a low generation rate, TTA is insignificant, so that all results approach the dotted line $T = G\tau a^{-3}/(1 + G\tau)$ for low G. For high G all results approach each other, pointing at a decreased significance of correlations. Large differences between the various results are observed for intermediate values of the
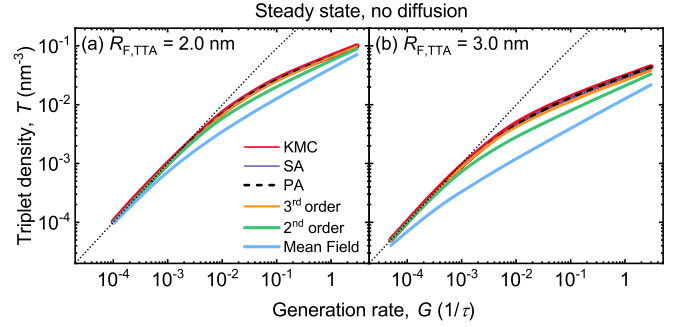
generation rate, where for realistic values $G\tau = 10^{-2}$ and $R_{F,TTA} = 3.0$ the MF result underestimates the triplet density by almost an order of magnitude. Apart from the MF and second-order approximations, the other approximations (third order, PA, SA) yield results in very good agreement with the benchmark KMC results.

Figure 6(a) shows, for $R_{F,TTA} = 3.0$ nm and $G\tau = 10^{-2}$, results for the pair correlation function $g(r)$ for the four main approximations, second order, third order, PA, and SA, in comparison to KMC results. The underestimation of the size of the depletion zone by the second-order approximation (green upward triangles) results in the underestimation of the triplet density by that approximation in Fig. 5. The third-order approximation (orange downward triangles) partly corrects for this underestimation and hence yields better results for the triplet density in Fig. 5. The PA correlation function, given by Eq. (39), describes the KMC correlation function quite well, with only a small difference at large distances [cf. Fig. 4(c)], while the SA yields an extremely good description. Figure 6(b) shows, in addition to results for $G\tau = 10^{-2}$ copied from Fig. 6(a), PA, SA, and KMC results for a larger triplet generation rate $G\tau = 10^{-1}$. The small deviation in $g(r)$ at large distances of the PA has increased somewhat,

FIG. 5. Dependence of the steady-state triplet density T, in the absence of triplet diffusion, on the triplet generation rate G for the various approximations of Sec. II, as compared to KMC results, for (a) $R_{F,TTA} = 2.0$ nm and (b) $R_{F,TTA} = 3.0$ nm. The dotted lines show the no-TTA limit $T = G\tau a^{-3}/(1 + G\tau)$.
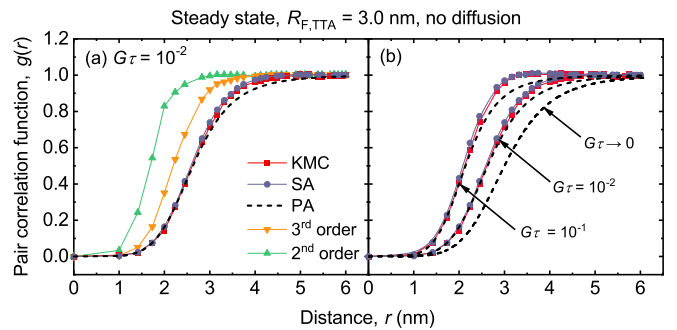

FIG. 6. (a) Steady-state triplet pair correlation functions $g(r)$ for $R_{F,TTA} = 3.0$ nm and $G\tau = 10^{-2}$ for the four main approximations in comparison to KMC results. (b) PA, SA, and KMC results for $g(r)$ for $G\tau = 10^{-1}$, $G\tau = 10^{-2}$ [same results as in (a)], and PA result for $G\tau \to 0$. Apart from the PA case, the data points have discrete values of r that are connected by straight lines.
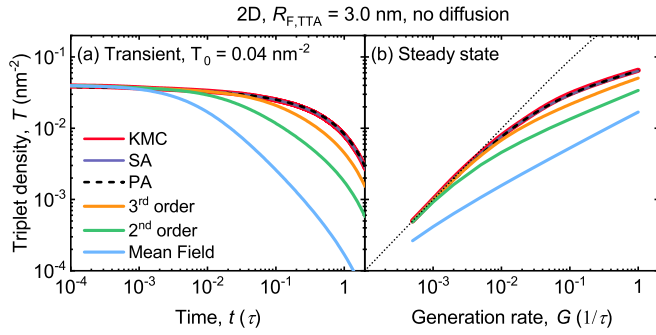
FIG. 7. (a) Transient triplet density $T(t)$ in two dimensions for the various approximations discussed in Sec. II, as compared to KMC results, for an initial triplet density $T_0 = 0.04$ nm^{-2} and $R_{F,TTA} = 3.0$ nm, in the absence of triplet diffusion. (b) Dependence of steady-state triplet density T in two dimensions, in the absence of triplet diffusion, on the triplet generation rate G for the various approximations, as compared to KMC results, for $R_{F,TTA} = 3.0$ nm. The dotted line shows the no-TTA limit $T = G\tau a^{-2}/(1 + G\tau)$.

while the SA still describes the KMC $g(r)$ very well. The reduction of the depletion zone for a larger generation rate leads to a decreased role of correlations and hence to the convergence of all results for high $G\tau$ observed in Fig. 5. The reason is that for high $G\tau$ the generation of triplets is so fast that there is insufficient time for the TTA process to generate correlations. We also added to Fig. 6(b) the result for the PA correlation function in the limit $G\tau \rightarrow 0$, which is $g(r) = 1/[1 + (R_{F,TTA}/r)^6]$, as obtained from Eq. (39) after putting $T = G\tau a^{-3}$. We have assumed thus far that triplets are generated homogeneously in three dimensions, either by photoexcitation or by electron-hole recombination. In practice, there are situations where triplets are generated in a 2D plane. This happens, for example, in thin emission layers or in situations where triplets are generated in the emission layer close to the interface with a charge transport layer. The latter can occur when one of the charge carriers in the emission layer has a much higher mobility than the other. For this reason, we also studied transient and steady-state triplet densities in a 2D square lattice. Analytical 2D results equivalent to the analytical 3D results can be found in Sec. II C. Figure 7(a) shows transient triplet densities for $R_{F,TTA} = 3.0$ nm and a 2D initial triplet density $T_0 = 4 \times 10^{-2}$ nm^{-2} for the five approximations discussed in Sec. II B. For this initial triplet density, the average number of triplets within a disk of radius $R_{F,TTA} = 3.0$ nm is 2.26, which is the same as the number of triplets within a sphere of this radius in the 3D case with $T_0 = 2 \times 10^{-2}$ nm^{-3}, which makes Fig. 7(a) comparable to Fig. 2(d). Figure 7(b) shows corresponding 2D steady-state results, which should be compared to Fig. 5(b). The general conclusions that we have drawn about the 3D results also hold for the 2D results. A noticeable difference, however, is that the effects of correlations in 2D are stronger than in 3D, which is, e.g., seen from the larger deviation of the MF results from the KMC results in the comparison of Figs. 7(a) and 7(b) to Figs. 2(d) and 5(b), respectively. This is in line with the well-known fact that in many-body theories correlations become more important in lower dimensions.
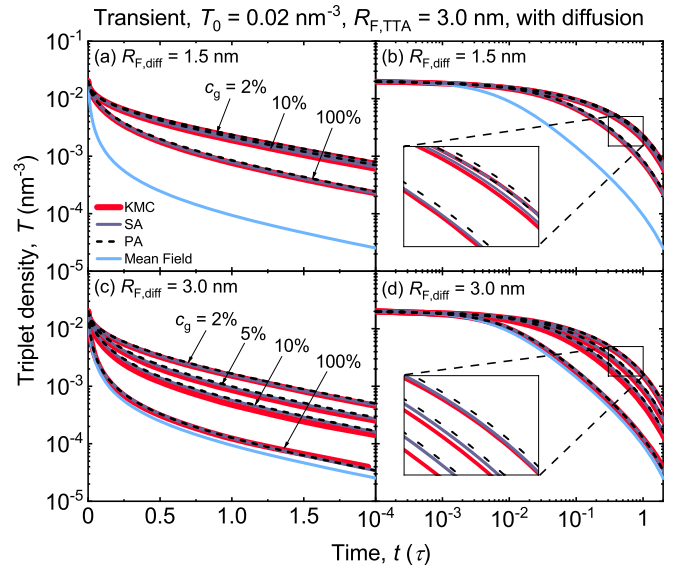

FIG. 8. Transient triplet density $T(t)$ for an initial triplet density $T_0 = 0.02$ nm^{-3}, $R_{F,TTA} = 3.0$ nm, and different guest concentrations c_g in the presence of triplet diffusion. (a) Transients for the mean-field approximation, the PA, and the SA as compared to KMC results, for $R_{F,diff} = 1.5$ nm. (b) Same as (a), but with a logarithmic time axis. (c) and (d) Same as (a) and (b), but for $R_{F,diff} = 3.0$ nm. The insets in (b) and (d) are magnifications of the indicated regions.

B. Triplet diffusion

In this subsection, we consider the effects of triplet diffusion on transient and steady-state triplet densities in the presence of TTA. Because triplets can only diffuse among phosphorescent guests, it is now important to distinguish between guest sites, on which the triplets can reside, and host sites, which we assume to be inaccessible to triplets. The approximate approach followed to account for this is explained in Sec. II D. This approach neglects percolation effects, where triplets can quickly diffuse along percolating pathways of guest molecules that happen to be close to each other. The approach therefore underestimates diffusion, but, as we will see, this underestimation is not severe.

Figure 8 shows, for $R_{F,TTA} = 3.0$ nm, an initial triplet density $T_0 = 0.02$ nm^{-3}, and various guest concentrations c_g, the transient triplet density $T(t)$ for $R_{F,diff} = 1.5$ nm [Figs. 8(a) and 8(b)] and $R_{F,diff} = 3.0$ nm [Figs. 8(c) and 8(d)]. We give results for the MF approximation, the PA, and the SA, in comparison to KMC results. For intermediate guest concentrations, like $c_g = 5$ and 10% in the case of $R_{F,diff} = 3.0$ nm, the SA and PA transients are lying slightly above the KMC transients, which is related to the fact that our approach is not able to fully capture the effects of percolation and underestimates diffusion. For 100% guest concentration, percolation effects are absent, explaining why for this case the PA and SA transients very closely follow the KMC transients. For low guest concentration, like $c_g = 2\%$, the role of diffusion becomes small, explaining why for low guest concentrations the PA and SA transients also very closely follow the KMC transients. As seen in the insets in Figs. 8(b) and 8(d), the SA transients are more accurate than the PA transients. The displayed MF transients are identical for both values of $R_{F,diff}$
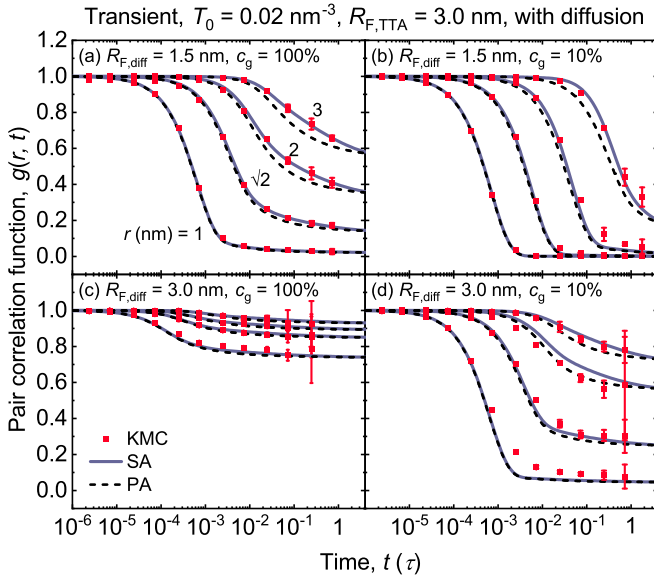
FIG. 9. Transient PA, SA, and KMC pair correlation functions $g(r, t)$ as a function of time for $T_0 = 0.02$ nm^{-3} and $R_{F,TTA} = 3.0$ nm in the presence of triplet diffusion, for (a) $R_{F,diff} = 1.5$ nm and $c_g = 100\%$, (b) $R_{F,diff} = 1.5$ nm and $c_g = 10\%$, (c) $R_{F,diff} = 3.0$ nm and $c_g = 100\%$, and (d) $R_{F,diff} = 3.0$ nm and $c_g = 10\%$. The error bars in the KMC results are obtained from results for different KMC runs.

and equal to the MF transient in Fig. 2(c) in the absence of diffusion. For $R_{F,diff} = 3.0$ nm and 100% guest concentration, diffusion is so fast that correlations are almost completely washed out (see below). As a result, the MF transient is close to the PA, SA, and KMC transients, as seen in Figs. 8(c) and 8(d).

A comparison of the transient PA and SA pair correlation functions with the KMC pair correlation functions $g(r, t)$ as a function of time for $R_{F,TTA} = 3.0$ nm, $T_0 = 0.02$ nm^{-3}, and four different values of r is shown in Fig. 9. Results are displayed for the four combinations $R_{F,diff} = 1.5$ and 3.0 nm, and $c_g = 100\%$ and 10%. A guest concentration of 10 mol% is typical for phosphorescent OLEDs. The case of 100% guest concentration could apply to single organic component fluorescent OLEDs, where the excitons are singlets instead of triplets. The results for the KMC correlation functions are given by the symbols, where the error bars are obtained from results for different KMC runs. In the case of $c_g = 10\%$ this includes KMC runs for different random locations of the guest sites in the simulation box. Because of the diffusion, there are much fewer triplets at later times in the simulation box than without diffusion. As a result, it is more difficult to obtain sufficient accuracy in the KMC correlation functions. We obtain a reasonable accuracy by performing an average of the correlation functions over finite time intervals. For this reason, results are shown for much fewer times than for the case without diffusion (Fig. 4).

In all cases, the PA and SA correlation functions in Fig. 9 are in quite good agreement with the KMC correlation functions. For 100% guest concentration [Figs. 9(a) and 9(c)] the PA correlation function deviates somewhat from the KMC correlation function, while the SA correlation function is very
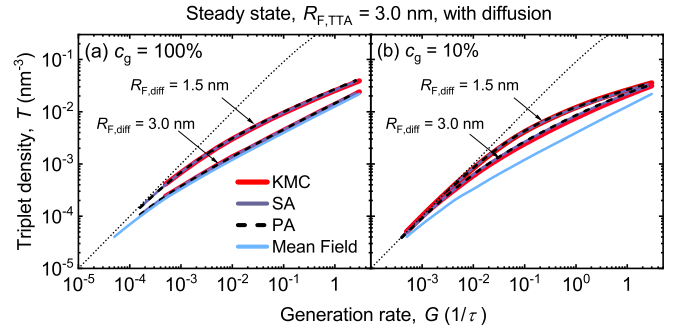
accurate. For 10% guest concentration [Figs. 9(b) and 9(d)] both the PA and SA correlation functions deviate somewhat from the KMC correlation functions, which should be attributed to the underestimation of diffusion by the neglect of percolation effects. The diffusion leads to incomplete depletion zones, with $g(r, t)$ initially dropping, but finally leveling off at nonzero values, as observed for $R_{F,diff} = 1.5$ nm and $c_g = 100\%$ in Fig. 9(a), and $R_{F,diff} = 3.0$ nm and $c_g = 10\%$ in Fig. 9(d). For $R_{F,diff} = 3.0$ nm and $c_g = 100\%$ the diffusion is so strong that the depletion zone has almost disappeared; see Fig. 9(c). This is the reason why the MF transient in Fig. 8(c) is so close to the PA, SA, and KMC transients. On the other hand, for $R_{F,diff} = 1.5$ nm and $c_g = 10\%$ diffusion is weak, leading to an almost completely developed growing depletion zone, see Fig. 9(b), as observed without diffusion in Fig. 4.

MF, PA, SA, and KMC steady-state results for the triplet density T as a function of the generation rate G for $R_{F,TTA} = 3.0$ nm, and $R_{F,diff} = 1.5$ and 3.0 nm, are shown in Figs. 10(a) and 10(b) for $c_g = 100\%$ and 10%, respectively. Corresponding PA, SA, and KMC pair correlation functions are given in Figs. 11(a) and 11(b) for generation rates $G = 10^{-1}\tau^{-1}$. For $c_g = 100\%$, both the PA and SA yield results in excellent agreement with the KMC results, both for the triplet densities
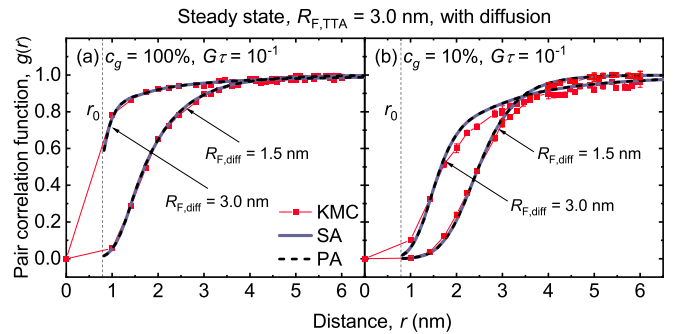

FIG. 10. Dependence of steady-state triplet density T on the triplet generation rate G for the mean field, PA, and SA approximation, as compared to KMC results, for $R_{F,TTA} = 3.0$ nm, and $R_{F,diff} = 1.5$ and 3.0 nm, for (a) 100% and (b) 10% guest concentration. The dotted lines show the no-TTA limit $T = G\tau a^{-3}/(1 + G\tau)$.

FIG. 11. Steady-state PA, SA, and KMC pair correlation functions $g(r)$ for $R_{F,TTA} = 3.0$ nm, $R_{F,diff} = 1.5$ and 3.0 nm, and $G\tau = 10^{-1}$ for (a) guest concentrations $c_g = 100\%$ and (b) $c_g = 10\%$. The KMC data points have discrete values of r and are connected by straight lines. For the PA and SA, $g(r)$ is a continuous function defined for $r > r_0 = 0.7929$ nm (see Sec. II D).

[Fig. 10(a)] and the correlation functions [Fig. 11(a)]. For $c_g = 100\%$ and $R_{F,diff} = 3.0$ nm, diffusion is so strong that even the MF result becomes reasonably accurate in Fig. 10(a), like in Figs. 8(c) and 8(d) for the transient case. In Fig. 11(a) we see that the correlations in this case are relatively unimportant. For $c_g = 10\%$ and $R_{F,diff} = 1.5$ nm the diffusion is weak and both the PA and SA results are very close to the KMC results and also very close to the results without diffusion in Fig. 5(b) (triplet densities) and Fig. 6(b) (correlation functions). For $c_g = 10\%$ and $R_{F,diff} = 3.0$ nm diffusion is important. The PA and SA results are then slightly above the KMC results in Fig. 10(b), because of the underestimation of diffusion by the neglect of percolation effects. The diffusion is, however, not strong enough to completely wash out correlations, as seen in Fig. 11(b). As a result, the MF result for the triplet density in Fig. 10(b) is not accurate. For $c_g = 10\%$ and $R_{F,diff} = 1.5$ nm diffusion is less important, leading to a more strongly deviating MF triplet density in Fig. 10(b) and a larger depletion zone in Fig. 11(b) as compared to $R_{F,diff} = 3.0$ nm.

IV. COMPUTATIONAL EFFICIENCY

In this section, we compare the computational efficiency of master equation calculations using the PA and SA to that of KMC simulations. We do not consider here the second- and third-order approximations, because these approximation are far less accurate than the PA and SA. We focus on a comparison for the transient calculations. In the case of steady-state calculations, the comparison is not straightforward because of the different procedures used to reach the steady state. The master equation calculations and KMC simulations were performed on comparable hardware (Intel Xeon Gold 6240 or comparable processors) with comparable numerical precision. The master equation calculations were done with Python codes that can be further optimized and possibly to some extent parallelized.

For the case of TTA without triplet diffusion, we only compare the CPU time for SA calculations, since an analytical expression is available for the PA [Eq. (33)]. As an example, we consider TTA with a Förster radius $R_{F,TTA} = 3.0$ nm. For the SA calculations the CPU time is independent of the initial triplet density T_0, as is expected, whereas the CPU time increases steeply with T_0 for the KMC simulations. For a typical initial triplet density $T_0 = 0.02$ nm^{-3}, the KMC simulations take for a single run already about a factor 4 longer than the SA calculations. The transient KMC results for this case, presented in Sec. III A, were obtained by averaging over 50–100 runs. The SA calculations, which obviously require only a single run, were in this case thus at least two orders of magnitude more time-efficient than the KMC simulations.

For the case with triplet diffusion, where also for the PA no analytical result is available, we compare the PA and SA calculation and KMC simulation times for $R_{F,TTA} = 3.0$ nm and $T_0 = 2\times10^{-2}$ nm^{-3} with $R_{F,diff} = 1.5$ and 3.0 nm, as a function of the guest concentration c_g. We find that the CPU time for the PA calculations is about three orders of magnitude smaller than for the SA calculations. For both approximations, the CPU time is about the same for $R_{F,diff} = 1.5$ and 3.0 nm and almost independent of c_g. For the KMC simulations, the CPU time increases approximately linearly with c_g and is

TABLE I. Overview of the methods for solving the master equation in the modeling of TTA discussed in this paper. Given are the equations solved and an assessment of the accuracy and feasibility of the calculations. Results of kinetic Monte Carlo (KMC) simulations serve as a benchmark.

	Exact	Mean-field (MF) approximation	Second-order approximation	Third-order approximation	Pair approximation (PA)	Superposition approximation (SA)
						Method
General equation(s)	Eq. (4) (general form) and Eq. (10) (coupled equations)	Eq. (12)	Eqs. (6),(8),(15)	Eqs. (6),(8),(9),(16)	Eqs. (19),(21)	Eqs. (19),(22)
Equation(s) transient triplet density (no diffusion)		Analytical: Eq. (28)	Numerical: Eqs. (6),(8),(15), putting $G = D_{kl} = 0$	Numerical: Eqs. (6),(8),(9),(16), putting $G = D_{kl} = 0$	Analytical: Eq. (33) (3D) and Eq. (35) (2D)	Numerical: Eqs. (23),(36), putting $G = 0$
Equation(s) steady-state triplet density (no diffusion)		Analytical: Eq. (37)	Numerical: Eqs. (6),(8),(15), putting $D_{kl} = 0$	Numerical: Eqs. (6),(8),(9),(16), putting $D_{kl} = 0$	Numerical: Eq. (42) (3D) and Eq. (44) (2D)	Numerical: Eqs. (23),(45)
Equation(s) transient and steady-state triplet density (with diffusion)		Same as no diffusion			Numerical: Eqs. (47),(48)	Numerical: Eqs. (47),(49)
Accuracy[a]	Perfect	Accuracy increases with increasing order, but is even for the third-order approx. often unsatisfactory			Accuracy is very close to that of KMC simulations; best for SA	
		Order of typical calculation times: MF< PA < second order ≈ SA << third order ≈ SA < KMC				
Feasibility of calculations[b]	Infeasible for systems with a realistic size					

[a] For the calculations without triplet diffusion (see, e.g., Fig. 2). When the role of diffusion increases, the added value of going beyond the mean-field approximation decreases (see, e.g., Fig. 8).

[b] For the calculations shown in Figs. 8(c) and 8(d) with $c_g = 10\%$. See Sec. III B.

considerably larger for $R_{\mathrm{F,diff}} = 3.0$ nm than for $R_{\mathrm{F,diff}} = 1.5$ nm. For a typical guest concentration $c_{\mathrm{g}} = 10\%$ the KMC simulations take for a single run with $R_{\mathrm{F,diff}} = 1.5$ nm about a factor 3 longer than the SA calculations, while this factor is an order of magnitude higher for $R_{\mathrm{F,diff}} = 3.0$ nm. For $R_{\mathrm{F,diff}} = 1.5$ nm, which may be considered as a realistic value for isoenergetic transfer between Ir-cored phosphorescent emitter molecules [17], KMC simulations for a typical number of 100 runs take at least two orders of magnitude longer than SA calculations. A further gain of three orders of magnitude can be obtained by making use of the PA, although this can slightly affect the accuracy; see Sec. III B.

We note that KMC simulation runs for different disorder configurations can be performed in parallel, which for the examples that were discussed above can reduce the wall time with respect to the CPU time by two orders of magnitude in the case of 100 single runs. The speed-up by using PA or SA calculations is nevertheless considerable and can be even further increased by optimizing and parallelizing the used codes.

V. SUMMARY, CONCLUSIONS AND OUTLOOK

We applied master equation modeling to the description of Förster-type triplet-triplet annihilation (TTA) in organic emission layers consisting of a guest phosphorescent emitter embedded in a host, without and with inclusion of Förster-type triplet diffusion among the emitter molecules. We derived from the master equation for the time dependence of the probabilities for the different states of the system a hierarchical chain of equations that includes all correlations in the positions of the triplets. Following the recent theoretical work on charge transport in disordered semiconductors [12], we solved this chain of equations by neglecting covariances higher than second or third order. However, we found that these approximations yield insufficiently accurate results.

Instead, we showed that using a low-triplet density pair approximation (PA) or the superposition approximation (SA)

yields accurate (PA) to very accurate (SA) results for relevant quantities, as benchmarked by kinetic Monte Carlo (KMC) simulations. This holds both for transient situations corresponding to time-resolved photoluminescence (TRPL) experiments as well as in steady-state situations. The CPU time required for the SA or PA calculations is, in some cases, orders of magnitude less than for the KMC simulations, which makes this type of master equation modeling an attractive alternative. In addition, this type of modeling provides important insight into the role of correlations in the process of TTA. Table I gives an overview of the methods used in this work, the equations solved, and an assessment of the accuracy and feasibility of the calculations.

With only one type of excitation (triplet excitons) present, this work can be considered as a pilot study for taking into account the complicating effects of correlations between excitations in accurate yet fast calculations of the photophysics of OLEDs. With the inclusion of charges, application to triplet-polaron quenching (TPQ) should be possible. We further foresee application to electron-hole recombination and to charge transport, where correlations caused by Coulomb interactions should be included, going beyond the methodology presented in Ref. [12]. With the further inclusion of energetic and positional disorder, a complete accurate and fast alternative to KMC simulations of the photophysics of OLEDs may become available.

[1] M. A. Baldo, D. F. O'Brien, Y. You, A. Shoustikov, S. Sibley, M. E. Thompson, and S. R. Forrest, Nature (London) **395**, 151 (1998).

[2] C. Adachi, M. A. Baldo, M. E. Thompson, and S. R. Forrest, J. Appl. Phys. **90**, 5048 (2001).

[3] C. Adachi, M. A. Baldo, S. R. Forrest, and M. E. Thompson, Appl. Phys. Lett. **77**, 904 (2000).

[4] M. A. Baldo, C. Adachi, and S. R. Forrest, Phys. Rev. B **62**, 10967 (2000).

[5] C. Murawski, K. Leo, and M. C. Gather, Adv. Mater. **25**, 6801 (2013).

[6] H. van Eersel, P. A. Bobbert, R. Janssen, and R. Coehoorn, Appl. Phys. Lett. **105**, 1561 (2014).

[7] H. van Eersel, P. A. Bobbert, and R. Coehoorn, J. Appl. Phys. **117**, 115502 (2015).

[8] R. Coehoorn, P. A. Bobbert, and H. van Eersel, Phys. Rev. B **96**, 184203 (2017).

[9] R. Coehoorn, P. A. Bobbert, and H. van Eersel, Phys. Rev. B **99**, 024201 (2019).

[10] F. Symalla, S. Heidrich, P. Friederich, T. Strunk, T. Neumann, D. Minami, D. Jeong, and W. Wenzel, Adv. Theor. Simul. **3**, 1900222 (2020).

[11] M. A. Bazrafshan, M. Ansari-Rad, and S. H. Pilehrood, Phys. Rev. B **101**, 094204 (2020).

[12] A. V. Shumilin and Y. M. Beltukov, Phys. Rev. B **100**, 014202 (2019).

[13] J. Cottaar and P. A. Bobbert, Phys. Rev. B **74**, 115204 (2006).

[14] N. N. Bogoliubov, J. Phys.-USSR **10**, 265 (1946).

[15] M. Born and H. S. Green, Proc. R. Soc. London, Ser. A **188**, 10 (1946).

[16] E. Lifshitz and L. Pitaevski, in *Course of Theoretical Physics*, edited by E. Lifshitz and L. Pitaevski, Course of Theoretical Physics Vol. 10 (Pergamon Press, Amsterdam, 1981), pp. 1–88.

[17] X. de Vries, P. Friederich, W. Wenzel, R. Coehoorn, and P. A. Bobbert, Phys. Rev. B **99**, 205201 (2019).

[18] J. G. Kirkwood, J. Chem. Phys. **3**, 300 (1935).

[19] J. G. Kirkwood and E. M. Boggs, J. Chem. Phys. **10**, 394 (1942).

[20] L. Monchick, J. Magee, and A. Samuel, J. Chem. Phys. **26**, 935 (1957).

[21] T. Waite, Phys. Rev. **107**, 463 (1957).

[22] https://simbeyond.com, the BUMBLEBEE software is provided by Simbeyond B.V.

[23] H. Matsuda, Phys. Rev. E **62**, 3096 (2000).

[24] Y. Zhang and S. R. Forrest, Chem. Phys. Lett. **590**, 106 (2013).

[25] E. Engel, K. Leo, and M. Hoffmann, Chem. Phys. **325**, 170 (2006).